Supporting Information

Ultracompact Computational Spectroscopy with a Detour-Phased Planar Lens

Wenkai Yang[1,2], Zijian Wang[1,2], Jian Xu[1,2], Dashan Dong[1,2], Guiyuan Cao[4], Han Lin[4], Baohua Jia[4], Lige Liu[1,2,*], Kebin Shi[1,2,3,*]

[1]State Key Laboratory for Mesoscopic Physics and Frontiers Science Center for Nano-optoelectronics, School of Physics, Peking University, Beijing 100871, China

[2]Collaborative Innovation Center of Extreme Optics, Shanxi University, Taiyuan 030006, China

[3]Peking University Yangtze Delta Institute of Optoelectronics, Nantong 226010, China

[4]Centre for Atomaterials and Nanomanufacturing, School of Science, RMIT University, Melbourne, 3000, VIC, Australia

*Correspondence: Lige Liu (lgliu@pku.edu.cn) and Kebin Shi (kebinshi@pku.edu.cn, telephone: 010-62768959).

Supplementary Material Note 1: Lens design based on the detour phase method

The detour phase method is a very convenient approach to control light within a single ultrathin interface. Phase modulation can be achieved by utilizing binary amplitude-only holograms based on the positions and sizes of an array of transmitted apertures on an opaque screen [Ref. S1]. This method was originally mainly used in computer-generated holography in the last century [Ref. S2 – Ref. S4]. With the optics research towards the microworld, it acquired more and more attentions and has recently been extended to fields such as meta-holograms [Ref. S5 – Ref. S7], nonlinear holography [Ref. S8, Ref. S9], and beam shaping [Ref. S10-Ref. S12]. Due to the circularly symmetric nature of lenses, we simplified this method to one dimensional and adopted it in ultrathin planar lens design by only considering grating distributions along the radial direction. The phase modulation of the graphene oxide (GO) lens based on the detour phased method is depicted in Fig. S1(a). When a plane wave with a grating period of Λ incident onto a grating, the transmitted light through the slits with a distance of D is diffracted along a certain angle θ:

$$\sin(\theta) = \frac{\lambda}{D} \tag{S1}$$

where λ is the working wavelength. However, for an adjacent slit with an offset of ΔD in a period (Fig. S1(a)), constructive interference along the angle θ is not satisfied, and the phase difference between them depends on their distance. This indicates that the desired phase shift between two adjacent slits can be modulated by shifting the spatial position:

$$\Delta\varphi = \frac{2\pi\Delta D}{\lambda}\sin(\theta) = \frac{2\pi\Delta D}{\Lambda} \tag{S2}$$

When the slit shift (ΔD) varies from 0 to Λ in each period, a phase shift between the adjacent slits covering the range from -π to π is obtained.

The center position of the m^{th} transparent ring is determined by the following equation when applying a specific phase distribution $\varphi(r)$ to the lens:

$$r_m = m\Lambda + \Lambda\varphi(r)/2\pi \tag{S3}$$

where Λ is the grating period, and for a convex lens, $\varphi(r)$ is the convergence phase distribution given by the function [S13]:

$$\varphi(r) = \frac{\pi r^2}{\lambda_d f_d} \tag{S4}$$

where λ_d and f_d are the designed working wavelength and focal length of the detour-phased lens, respectively. The focusing is a result of the constructive interference of wavelets transmitted through different rings as depicted in Fig. S1(b). The fixed linewidth of the transparent rings distinguishes the detour phase design from the traditional Fresnel zone plate, in which the width of the alternating transparent and opaque zones decreases farther from the center.

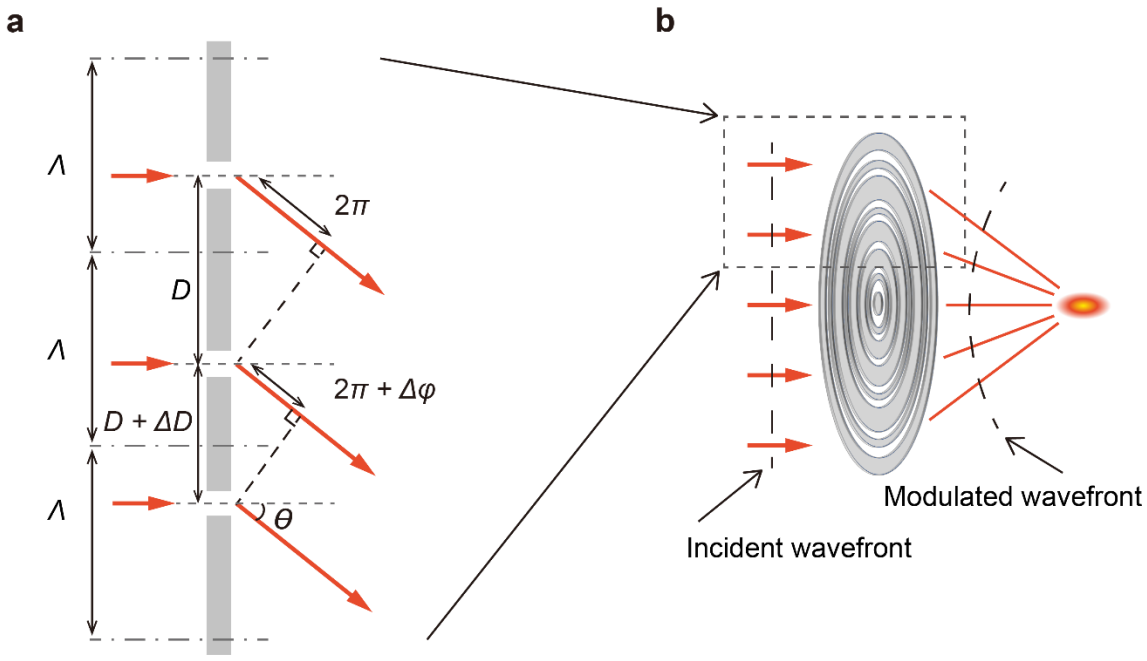

Fig. S1. GO planar lens design based on detour phase method. (a) Schematic illustration of detour phase modulation rule for arbitrary wavefront shaping. (b) Focusing due to constructive interference of wavelets in a GO planar lens.

Supplementary Material Note 2: Focusing fields calculation

The intensity distribution of the focusing fields of the GO lens is calculated using the Fresnel scalar diffraction theory with a circular symmetry as:

$$U_2(r_2,z)=\frac{\mathrm{i}2\pi}{\lambda z}\exp(-\mathrm{i}kz)\exp\left(-\frac{\mathrm{i}kr_2^2}{2z}\right)\int U_1^{'}(r_1)\exp\left(-\frac{\mathrm{i}kr_1^2}{2z}\right)J_0\left(\frac{kr_1r_2}{z}\right)r_1\mathrm{d}r_1 \quad \text{(S5)}$$

where the subscripts '1' and '2' indicate the parameters in the lens plane and in the focal plane, respectively, r is the perpendicular distance to the optics axis and z is the distance to the lens surface along the optics axis, $k=\lambda/2\pi$ is the wave vector of the light, $U_1^{'}(r_1)$ is the light field after the detour-phased lens, and can be calculated as:

$$U_1^{'}(r_1)=U_1\cdot t(r_1) \quad \text{(S6)}$$

where U_1 is the incident light field and t is the modulation induced by the detour-phased lens. As a result, intensity distributions behind the lens at different lateral (r_2) and axial (z) positions can be calculated using Eq. S5 and Eq. S6.

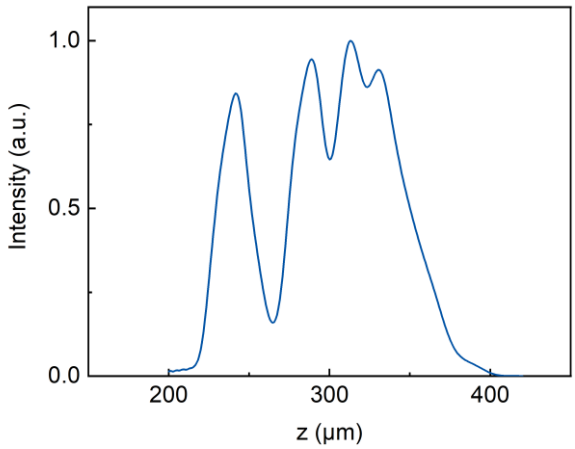

Figure S2. Simulated intensity distribution of the input spectrum after the GO lens.

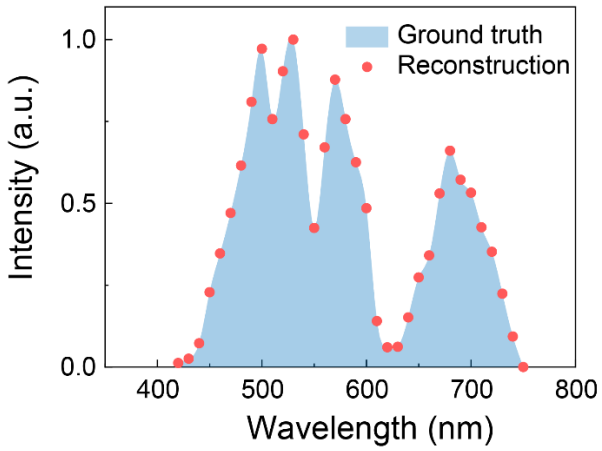

Fig. S3. Spectrum reconstruction at a wavelength interval of 10 nm. Original () and reconstructed (red dotted line) spectrum.

Supplementary Material Note 3: Spectrum reconstruction capability analysis.

The principle of the GO micro-spectrometer in this work is based on the strong axial chromatic dispersion of diffractive lenses, which can be expressed as:

$$f = \frac{\lambda_d f_d}{\lambda} \tag{S7}$$

where λ_d and f_d represent the designed wavelength and the designed focal length, respectively.

The resolution is limited by diffraction when not using the computational method, and Rayleigh criterion is generally used for determination of the resolving power [S14]. When a monochromatic plane wave near the design wavelength irradiated the lens, the intensity distribution of the longitudinal focal field on the axis is expressed by:

$$I = \left[\frac{\sin(u/4)}{u/4} \right]^2 \tag{S8}$$

where u can be expressed as:

$$u = \frac{2\pi}{\lambda} \left(\frac{a}{f} \right)^2 \Delta z \tag{S9}$$

where a is the lens radius, Δz is the distance from the focal point. Thanks to the detour-phased design, aberration-free diffraction-limited focal spots are obtained along the optical axis when a series of monochromatic plane waves with various wavelengths illuminate the GO planar lens. With Rayleigh criterion, diffraction-limited resolution is achieved when the center of one diffraction pattern is directly over the first minimum of the other. As a result, the corresponding

minimum distance between two spots along the optical axis is $\Delta z_{min} = f_1 - f_2$ when $u/4=\pi$ from Eq. S8, where f_1 and f_2 represent the focal lengths of two consecutive wavelengths, respectively.

When Δz_{min} in Eq. S9 is substituted with $\Delta\lambda$ using Eq. S7, the resolving power of GO lenses can be obtained:

$$\frac{\lambda}{\Delta\lambda} = \frac{a^2}{2f\lambda} \tag{S10}$$

As a result, the resolving power is proportional to the lens aperture a, and inversely proportional to the focal length f. Additionally, because of the strong anomalous dispersion properties of the detour-phased GO lens, the width of the focal point along the optical axis is inversely proportional to the incident wavelength, that is, poor resolution at shorter wavelength. When using the GO lens parameters in this work (λ_d = 550 nm, f_d = 300 μm, a = 200 μm), the resolving power is calculated to be 30.3, and the resolution required for measuring a spectrum covering 420-750 nm is calculated to be 24.75 nm.

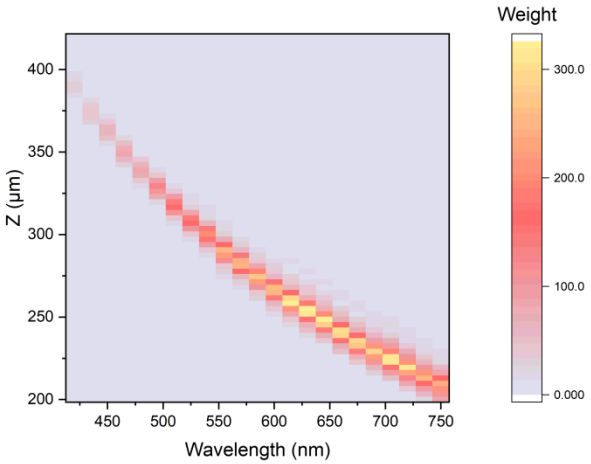

Figure S4. Surface plot for the experimentally measured mapping matrix.

Supplementary Material Note 4: Spectrum reconstruction in the infrared band.

GO material possesses nearly uniform optical properties across a relatively wide band from 400 nm to 1700 nm where both refractive index and extinction coefficient are almost maintained. This means our detour-phased lens using GO material is able to achieve efficient focusing across the whole range.

As a result, we designed a new detour-phased GO planar lens with a working wavelength of 1200 nm, a focal length (f) of 300 μm, and a lens radius (R) of 100 μm. The resulting numerical aperture is equal to the one used in the main text (NA = 0.32). The intensity distribution along the optical axis in the focal region of the planar lens was calculated using the Fresnel scalar diffraction theory. The focal length variances resulted from the axial chromatic dispersion of the detour-phased planar lens was shown in Fig. S5(a) at the incident wavelengths of 900 nm, 1200 nm and 1500 nm, respectively. The corresponding lens profile is presented in Fig. S5(b). An incident beam with a broadband random spectrum (900 - 1500 nm) was used to demonstrate the validity of the spectrum reconstruction method in infrared range. The corresponding axial intensity distribution behind the detour-phased lens was calculated using Fresnel diffraction theory. Spectrum reconstruction accuracy (ratio of the accurately retrieved points) at various wavelength intervals are investigated as in the visible range, and the results are shown in Fig. S5(c). It can be seen that our computational method shows similar tendency as it in the visible range expect for the minimum wavelength interval that can be distinguished moves to 18 nm. This is reasonable because longer wavelength leads to larger focal point, resulting in the resolution decreasing compared with that in visible (Focal point along the optical axis can be estimate using 2*lambda^2/NA).

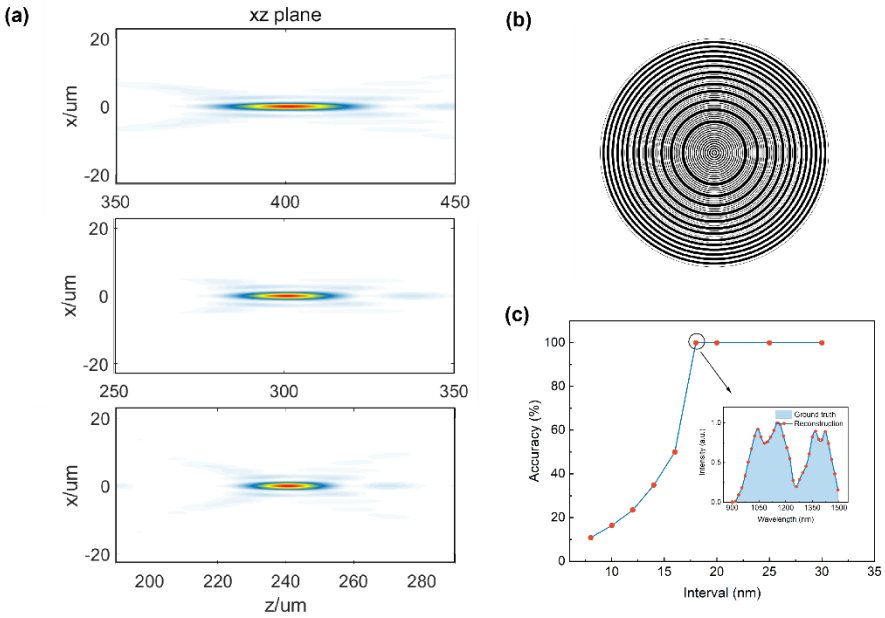

Figure S5. Simulation of the detour-phased lens-based micro-spectrometer in the infrared range. a. Longitudinal intensity distributions at 900 nm, 1200 nm, and 1500 nm incidence. b. Theoretically calculated lens profile with unevenly spaced concentric rings. c. Spectrum reconstruction accuracy with wavelength intervals from 8 nm to 30 nm. Inset: spectrum reconstruction with a wavelength interval of 18 nm, where solid blue region and red dotted line are the original and reconstructed spectrum, respectively.

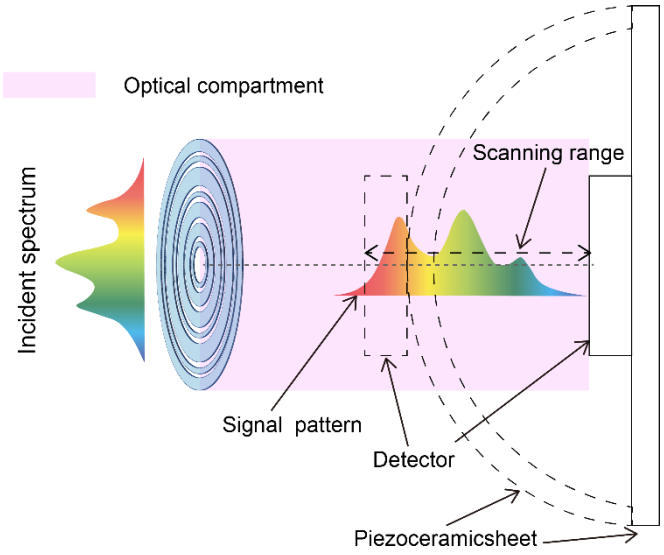

Figure S6. Schematic illustration of the micro-spectrometer using piezo device. Pink zone refer to the optical compartment.

Supplementary Material Reference:

[S1] B. R. Brown, A. W. Lohmann. Complex spatial filtering with binary masks. Applied Optics **5**, 967-969 (1966).

[S2] A. W. Lohmann and D. P. Paris, Binary Fraunhofer holograms, generated by computer. Applied Optics 6, 1739-1748 (1967).

[S3] W. H. Lee, Binary computer-generated holograms. Applied Optics, 18, 3661-3669 (1979).

[S4] C. K. Hsueh and A. A. Sawchuk, Computer-generated double-phase holograms. Applied Optics, 17, 3874-3883 (1978).

[S5] M. Khorasaninejad, A. Ambrosio, P. Kanhaiya, et al. Broadband and chiral binary dielectric meta-holograms. Science Advances, 2, e1501258 (2016).

[S6] C. Min, J. Liu, T. Lei, et al. Yuan, Plasmonic nano-slits assisted polarization selective detour phase meta-hologram. Laser Photonics Review, 10, 978-985 (2016).

[S7] Z. Deng, M. Jin, X. Ye, et al. Full-color complex-amplitude vectorial holograms based on multi-freedom metasurfaces. Advanced Function Materials, 30, 1910610 (2020).

[S8] P. Chen, C. Wang, D. Wei, et al. Quasi-phase-matching-division multiplexing holography in a three-dimensional nonlinear photonic crystal. Light: Science & Applications, 10, 146 (2021).

[S9] B. Wang, X. Hong, K. Wang, et al. Nonlinear detour phase holography. Nanoscale, 13, 2693-2702 (2021).

[S10] W. K. Yang, L. G. Liu, D. S. Dong, et al. Detour-phased perovskite ultrathin planar lens using direct femtosecond laser writing. Photonics Research, 10, 2768-2777 (2022).

[S11] A. Zhao, A. Pham, and A. Drezet, Plasmonic fork-shaped hologram for vortex-beam generation and separation. Optics Letters, 46, 689-692 (2021).

[S12] S. Wei, G. Cao, H. Lin, et al. High tolerance detour-phase graphene-oxide flat lens. Photonics Research, 9, 2454-2463 (2021).

[S13] J. Albero, J. A. Davis, D. M. Cottrell, C. E. Granger, K. R. McCormick, and I. Moreno, Generalized diffractive optical elements with asymmetric harmonic response and phase control. Applied Optics **52**, 3637-3644 (2013).

[S14] M. Born, and W. Emil. Principles of optics: electromagnetic theory of propagation, interference and diffraction of light. Elsevier, 2013.